Characterization of the Excited States Responsible for the Action of Silver(I)-Doped ZSM-5 Zeolites as Photocatalysts for Nitric Oxide Decomposition

Sofian M. Kanan, Mohammad A. Omary, and Howard H. Patterson*

Department of Chemistry, University of Maine, Orono, Maine 04469

Masaya Matsuoka and Masakazu Anpo

Department of Applied Chemistry, College of Engineering, University of Osaka Prefecture, Sakai, Osaka 599-8531, Japan

Received: July 30, 1999; In Final Form: January 17, 2000

Ag(I)/ZSM-5 catalyst was prepared and characterized spectroscopically in relation to its photocatalytic reactivity for the photodecomposition of nitric oxide. UV irradiation of the Ag(I)/ZSM-5 catalyst in the presence of NO leads to efficient catalytic conversion of NO into N_2, O_2, and other nitrogen oxides. Emission and synchronous-scan photoluminescence spectra indicate the presence of several environments for the Ag(I) ions in the ZSM-5 host. Ground- and excited-state electronic structure calculations for models in which $[Ag^+]_n$ ions ($n \geq 1$) are coordinated to NO molecules, suggest that N−O bonds are stronger in the ground state while N−N and O−O bonds are stronger in certain excited states. The luminescence and molecular orbital data suggest that more than one catalytic site for the photodecomposition of NO is present in Ag(I)/ZSM-5. The results of EXAFS have been used in support of the excited-state assignments.

Introduction

The design of photocatalysts encapsulated within zeolites is a promising approach for the development of photocatalysts that effectively catalyze the decomposition of toxic agents in the atmosphere such as NO_x. Zeolites can be tailored for specific actions by suitable synthetic conditions. The design of highly efficient and selective photocatalysts that utilize solar energy through chemical storage with minimum energy loss is of vital interest. The preparation and characterization of supported zeolites have been extensively studied in the last two decades. Examples of the support include titanium,[1−11] vanadium,[12−14] and molybdenum[15,16] oxides, and Ag(I)[17−20] and/or Cu(I)[21−29] ions. The Cu(I) ion-exchanged ZSM-5 samples have shown specific activity for the catalytic decomposition of nitrogen oxides NO_x, even with a high concentration of oxygen and sulfur oxides.[30−34] The photocatalytic activity of Cu(I)/ZSM-5 for NO_x decomposition is higher than that of V_2O_5/TiO_2.[28] The photocatalytic reactivity of Cu(I)/ZSM-5 catalysts has been found to be strongly affected by the local structure of the Cu(I) ions, which could easily be modified by changing the type of zeolite and the loading of the copper(I) ion.[21] Photoluminescence studies of the catalysts have suggested that the Cu(I) ions anchor onto the ZSM-5 and form isolated copper species near Brönsted sites in the zeolite.[28]

Recently, it has been reported that Ag(I)/ZSM-5 catalysts have several advantages over Cu(I)/ZSM-5 in their action as photocatalysts for the direct decomposition of NO.[12,17−18] First, Ag(I)/ZSM-5 has shown higher photocatalytic reactivity than Cu(I)/ZSM-5. For example, the rate of NO_x decomposition per exchanged cation of the Ag(I)/ZSM-5 catalyst is 10 times faster than the corresponding rate for Cu(I)/ZSM-5.[23,35] This reactivity can be attributed to the high chemical stability of the silver ion and the efficient interaction of the excited electronic state of the silver ion with NO.[20,22] Also, the Cu(I)/ZSM-5 catalyst loses its photocatalytic reactivity in the presence of O_2, while Ag(I)/ZSM-5 maintains its reactivity even in the presence of oxygen and water.[23] Furthermore, the pretreatment of Ag(I)/ZSM-5 can be carried out at lower temperatures than those needed for the pretreatment of Cu(I)/ZSM-5. Understanding the electronic structure of the Ag(I)/ZSM-5 catalyst is central for further advances in this field.

Silver(I) materials have been studied extensively in the literature by spectroscopic techniques in order to elucidate fundamental issues in chemistry, such as closed-shell Ag−Ag interactions, and to study their roles in technological applications such as photographic materials, semiconductors, and photocatalysts. The materials studied included coordination compounds,[36−41] halides,[42−45] and oxides of Ag(I).[46−48] Recent examples include $Tl[Ag(CN)_2]$ and $[Ag(CN)_2^-]$/KCl.[40,41] The photoluminescence bands of these species have been explained in terms of excited-state Ag−Ag interactions leading to exciplex formation.[40,41] The formation of exciplexes is less well-known in inorganic compounds relative to organic compounds.[49] Only a few examples are known in which exciplexes are metal−metal bonded. Zink et al. have reported the formation of $*[Cu-Cu]^{2+}$ and $*[Cu-Ag]^{2+}$ exciplexes in β"-alumina.[50] The formation of $*[Ag_n]^{n+}$ excimers and exciplexes in oxide environments have not been reported prior to this study, to our knowledge. Recently, the formation of Ag−Ag bonded exciplexes has been reported in the $[Ag(CN)_2^-]$/KCl system. Excimers and exciplexes form between adjacent $[Ag(CN)_2^-]$ ions in a KCl lattice, giving rise to several luminescence bands in the 285−610 nm range.[41] It is one objective of this study to investigate the possible role of exciplex formation in the photocatalytic activity of Ag(I)-doped ZSM-5 zeolites for the decomposition of nitric oxide.

In the present work, we report a low-temperature luminescence study at 11 K of ZSM-5 zeolite anchored with Ag(I) ions. Previous spectroscopic studies on this system have reported the

10.1021/jp992703c CCC: $19.00
Published on Web 03/29/2000

presence of a single emission band at 77 K that was assigned to the radiative transition $4d^9 5s^1 \rightarrow 4d^{10}$ of the Ag(I) ion.[18,23] The study herein indicates the presence of several luminescence bands. A detailed assignment of the luminescent excited states is presented and discussed in comparison with previous assignments in the literature. The luminescence peaks in the emission and synchronous-scan spectra herein are related to the presence of different $[Ag_n]^{n+}$ oligomeric sites in the ZSM-5 zeolite. The photodecomposition of NO on the Ag(I)/ZSM-5 catalytic surface is modeled by molecular orbital calculations, which underscore the significance of Ag−Ag bonding for the photocatalytic reactivity of the Ag(I)-doped ZSM-5 zeolite.

Experimental Section

Ag(I)/ZSM-5 ($SiO_2/Al_2O_3 = 23.3$) catalyst was prepared by ion-exchange with $Ag(NH_3)_2^+$. Silver loading is around 2.5 wt % as metal. The silver loading of the sample was determined to be 6.7 wt % after drying at 375 K in air. Before spectroscopic measurements were recorded, the sample was treated as follows: degassed at 295 K for 1 h, calcined at 675 K in the presence of 20 Torr of O_2 for 1 h, and then degassed at 475 K for 1 h. The sample was immediately sealed in quartz glass tubing with an oxygen−acetylene torch.

Photoluminescence spectra were recorded with a PTI spectrofluorometer equipped with two excitation monochromators and a 75 W xenon lamp. Excitation and synchronous-scan spectra were corrected for variations in lamp intensity using the quantum counter rhodamine B. The spectra were recorded as a function of temperature, using liquid helium as the coolant in a model LT-3-110 Heli-Tran cryogenic liquid transfer system equipped with a temperature controller. Extended X-ray absorption fine structure (EXAFS) studies were carried out at the BL-10B facility of the Photon Factory at the National Laboratory for High-Energy Physics, Tsukuba, Japan. The normalized spectra were obtained by procedures described in previous papers[51] and Fourier transformation was performed on k^3-weighted EXAFS oscillations in the range of 3−12 $Å^{-1}$. Curve fitting of the EXAFS data was carried out by employing the iterative nonlinear least-squares method of Levernberg[51] and the empirical backscattering parameter sets extracted from the shell features of silver compounds.

Computational Details

Extended Hückel molecular orbital calculations were performed using the FORTICON 8 program (QCMP011). This program allows for excited-state calculations. The calculations have been performed for the models shown in Chart 1. The parameters and interatomic distances used are summarized in Table 1.[52,53] Restricted Hartree−Fock ab initio calculations were carried out using the STO-3G basis set available in SPARTAN (Version 4.1.1, Wave function Incorporated, Irvine, California).

Results

1. Characterization of the Ag(I)-Doped ZSM-5 Catalyst. *1.1. Photoluminescence Spectra*. Figure 1 shows the emission spectra of Ag(I)/ZSM-5 at 11 K. The emission spectra are strongly dependent on the excitation wavelength. We label the three major luminescence bands as A, B, and C, as shown in Figure 1. Each of these bands becomes dominant over the others by selecting a characteristic excitation wavelength. Excitation peaks at ca. 220−240, 250−270, and 280−300 nm are observed upon monitoring the emission at the maxima shown in Figure 1. Therefore, the different emission bands are resolved by site-selective excitation. An inspection of the luminescence spectra in Figure 1 illustrates the presence of some structure within the major emission bands. For example, band B contains peaks at ca. 310, 330, and 345 nm.

CHART 1

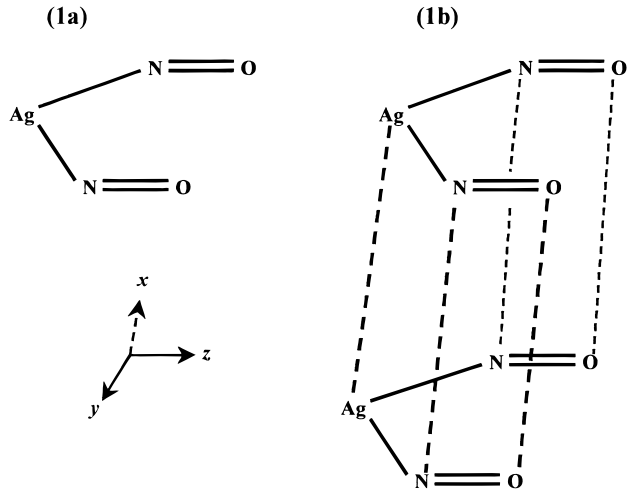

TABLE 1: Parameters Used in Extended Hückel Calculations[a,b]

atom	orbital	H_{ii} (eV)	ξ	interatomic distance, Å	
Ag	4d	−13.91	3.248	N−O	1.20
	5s	−6.453	1.594	Ag−(NO)[c]	2.653
	5p	−3.289	1.170		
N	2s	−26.25	1.886		
	2p	−13.83	1.728		
O	2s	−34.02	2.192		
	2p	−16.77	2.018		

[a] Orbital energies and wave functions are taken from ref 52. [b] Interatomic distances are taken from ref 53. [c] The Ag−(NO) distance here refers to the *z*-component of the Ag−N bond (see Chart 1), as the *y*-component was varied in the calculations. This value is modified from the Cu−N distance in ref 53 after accounting for the difference in the ionic radii between Ag(I) and Cu(I) ions.

Synchronous-scan luminescence spectroscopy is utilized in this study because the method has special advantages in studying chemical systems in which more than one luminophore is present. It is possible to see luminescence spectra for weakly luminescent compounds in the presence of other luminescent species. This method involves locking the excitation and emission wavelength drives together at a constant wavelength difference ($\Delta\lambda$) and recording the luminescence intensity while scanning the UV−visible region of the spectrum.[54,55] Synchronous-scan luminescence spectra have more defined peaks as compared to "normal" luminescence spectra (emission and excitation). The synchronous-scan method has been applied for the isolation of organic compounds even at low concentrations,[54,56] whereas inorganic materials have not been investigated extensively using this method, to our knowledge. The intensity of a synchronous-scan peak is given by the following relation:

$$I_S(\lambda) = k\, I_m(\lambda)\, I_x(\lambda - \Delta\lambda) \qquad (1)$$

where I_S is the synchronous-scan luminescence intensity, k is a constant, $I_m(\lambda)$ and $I_x(\lambda - \Delta\lambda)$ are the emission and excitation intensities as functions of the emission and excitation wavelengths, respectively. Equation 1 can be rewritten as

$$I_S(\lambda) = k'\, \phi(\lambda)\, I_0(\lambda - \Delta\lambda)\, \alpha_L(\lambda - \Delta\lambda)\, \Delta x\, \Delta y \qquad (2)$$

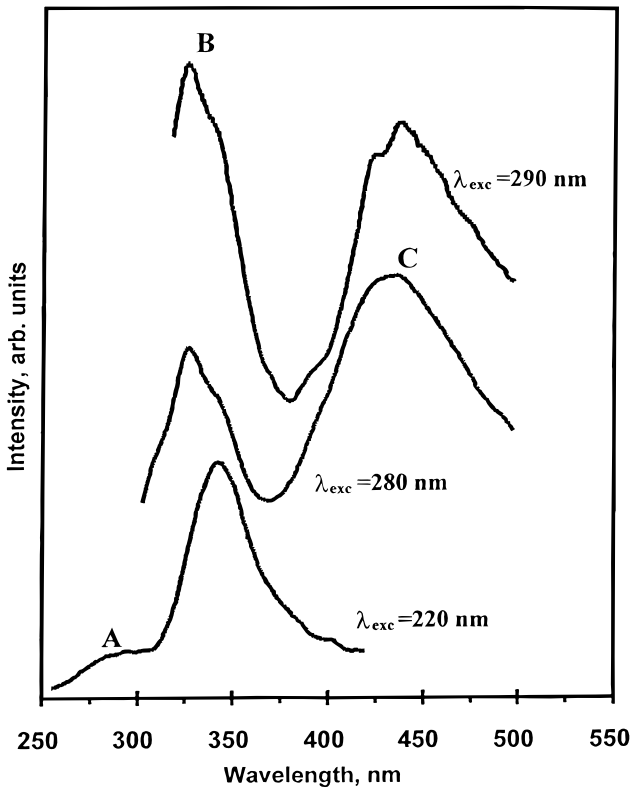

Figure 1. Emission spectra of Ag(I)/ZSM-5 at 11 K with the different excitation wavelengths as indicated. Relative intensities between the different spectra are not comparable.

where k' is a proportionality constant, $\phi(\lambda)$ is the luminescence quantum yield of the luminophore at the emission wavelength, I_0 is the intensity of the excitation source (the xenon lamp) at the excitation wavelength ($\lambda - \Delta\lambda$), α_L is the product of the luminophore's extinction coefficient and concentration, and Δx and Δy are the widths of the emission and excitation beams, respectively. The major excitation bands of the Ag(I)/ZSM-5 system are in the UV region ($\lambda_{exc} < 300$ nm), where the intensity of the xenon lamp decreases sharply relative to the lamp intensity at longer wavelengths. Therefore, it is important to eliminate the dependence of I_S on I_0. We have used the quantum counter rhodamine B to correct the synchronous-scan signals for variations in the lamp intensity. Therefore, the corrected synchronous-scan signal (I_S') can now be written as

$$I_S'(\lambda) = K\,\phi(\lambda)\,\alpha_L(\lambda - \Delta\lambda) \qquad (3)$$

where K is a constant that includes the slit-widths, which were held constant during the synchronous-scan measurements. Hence, the corrected synchronous-scan signal used herein is a function of only ϕ and α_L, which are intrinsic properties of the luminophore.

Figure 2 shows the synchronous-scan luminescence spectra of the Ag(I)/ZSM-5 catalyst at 11 K as a function of $\Delta\lambda$. The spectra show many resolved peaks, some of which are labeled as A−F in Figure 2. It is obvious that the synchronous-scan method has enabled us to see more luminescence peaks than the conventional emission spectra. For example, the shoulder that appeared at ∼280 nm in the emission spectra in Figure 1 becomes more distinct in the synchronous-scan spectrum in Figure 2. The longer-wavelength emission peaks in the ∼500−700 nm region (Figure 2) were not evident in the conventional emission spectra. Peaks in the synchronous-scan spectra appear with their maxima at different $\Delta\lambda$ values. This can be explained by considering that different Ag species on the ZSM-5 substrate have different Stokes shifts.

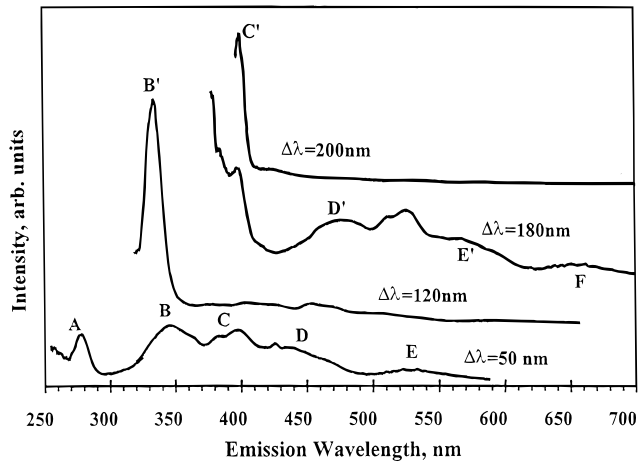

Figure 2. Synchronous-scan photoluminescence spectra of Ag(I)/ZSM-5 at 11 K using different values of $\Delta\lambda$. Relative intensities between the different spectra are not comparable.

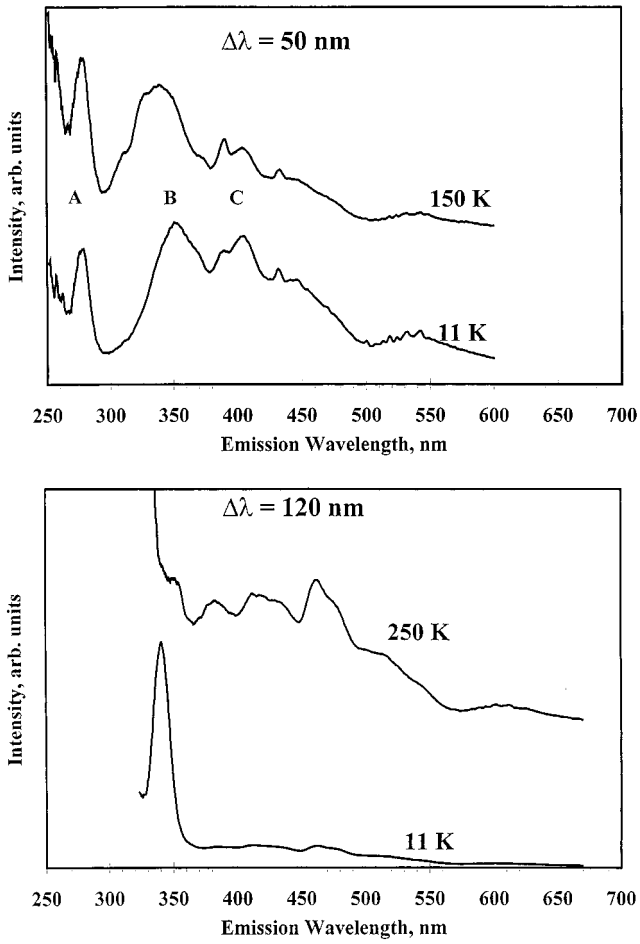

Figure 3. Synchronous-scan photoluminescence spectra of Ag(I)/ZSM-5 as a function of temperature with $\Delta\lambda$ of 50 nm (a) and 120 nm (b). Relative intensities between the different spectra are not comparable.

Figure 3 illustrates the effect of temperature on the synchronous-scan luminescence spectra of Ag(I)/ZSM-5 catalyst. An increase in temperature leads to a change in the relative intensities of the peaks within individual luminescence bands, as illustrated in Figure 3a using $\Delta\lambda$ of 50 nm. A more drastic example is shown in Figure 3b using $\Delta\lambda$ of 120 nm. In this example, an increase in temperature leads to a large reduction

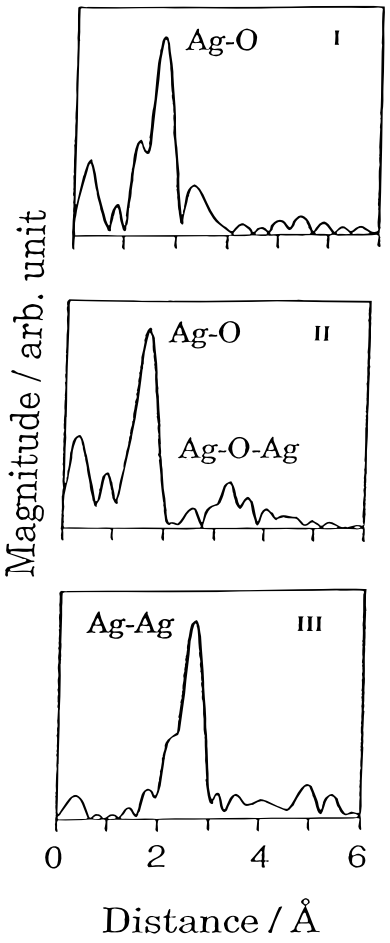

Figure 4. FT-EXAFS spectra of the Ag(I)/ZSM-5 catalyst (**I**), Ag_2O powder (**II**), and a Ag foil (**III**). The spectra are not corrected for phase shifts.

in the relative intensities of the higher-energy bands accompanied with an increase in the relative intensities of the lower-energy bands, which become distinct at 250 K.

1.2. EXAFS Measurements. Figure 4 shows the FT-EXAFS spectra of the Ag(I)-doped ZSM-5 catalyst (I), bulk Ag_2O (II), and Ag foil (III), respectively. The EXAFS spectrum of Ag_2O shows peaks at around 1.8 and 3.5 Å, while silver foil exhibits a peak at ~2.5 Å (values shown are uncorrected for phase shift). The corresponding crystallographic values have been reported in structural studies near 2.1, 4.1, and 2.9 Å, respectively.[57−59] The peaks in Figure 4 appear at shorter distances than the crystallographic values due to the photoelectron phase shift arising from the scattering processes. The EXAFS spectrum of the Ag(I) ZSM-5 catalyst shows distinct peaks in the regions of the 1.8 Å peak of Ag_2O and the 2.5 Å peak of Ag foil.

2. Electronic Structure Calculations. The luminescence and EXAFS data in this study suggest the presence of Ag_n^{n+} oligomers in the Ag(I)/ZSM-5 lattice. Furthermore, a recent study by Anpo et al. has demonstrated remarkably high photocatalytic reactivity for the decomposition of NO on Ag(I)/ZSM-5 surfaces, with decomposition rates approximately 10 times faster than those on Cu(I)/ZSM-5 surfaces (which were known to be the most efficient catalyst for NO decomposition).[18] These facts have lead us to hypothesize that the photocatalytic activity of Ag(I)/ZSM-5 zeolites for the decomposition of NO may be enhanced by the presence of different Ag_n^{n+} oligomeric sites in the zeolite host. This hypothesis has been tested by carrying out a series of ab initio and extended Hückel calculations for monomer and dimer models of Ag(I) ions interacting with NO molecules. The models selected were designed to examine the potentiality for Ag(I) monomers and oligomers to photocatalyze the reaction:

$$2NO + h\nu \xrightarrow{[Ag^+]_n} N_2 + O_2 \qquad (4)$$

The monomer model has two NO molecules adsorbed on a Ag(I) ion in a V-shaped C_{2v} geometry (Chart 1a). The dimer model has two Ag(I) ions adjacent to each other, each has two NO molecules adsorbed on it in a V-shaped C_{2v} geometry (Chart 1b).

Figure 5 shows the electronic structure of the monomer model after minimization by extended Hückel calculations. We recognize three types of transitions in this analysis: intra-ligand transitions, transitions between metal orbitals, and metal-to-ligand charge transfer (MLCT) transitions. The HOMO → LUMO transition is an intraligand transition between the molecular orbitals of the NO molecules. This transition is forbidden by symmetry for an electric dipole transition and is not studied herein. Other intraligand transitions originate from low-lying NO orbitals (not shown in Figure 5) to the vacant NO orbitals shown in Figure 5. These transitions have extremely high energies and, hence, are not pursued further. On the other hand, the lowest-energy transition between metal orbitals is the HOMO-1 → LUMO+3 transition, which represents a 4d−5s transition of the Ag(I) ion. The energy of this transition in the minimized structure of the $Ag(NO)_2^+$ model is very high (8.06 eV) and even higher than the energy of the same transition in the Ag(I) free ion (see Table 1) by about 0.6 eV ($\sim 5 \times 10^3$ cm^{-1}). Furthermore, the calculations herein show that the two electronic states involved in this transition have a virtually pure Ag character (97% and 98%, respectively) with infinitesimal contribution from the NO orbitals. Therefore, the 4d−5s transition is not expected to lead to any change in the bonding properties of NO molecules adsorbed on Ag(I) ions according to extended Hückel calculations. This leaves the MLCT transitions as the only transition type that will likely lead to the photoreaction described in eq 4. Such transitions are both strongly allowed by symmetry for electric dipole transitions and have low energies that are accessible by common light sources in the near-UV and visible regions.

Two MLCT transitions have been studied: the HOMO-1 → LUMO transition, and the HOMO-1 → LUMO+2 transition. We shall refer to these transitions as MLCT1 and MLCT2, respectively (labeled in Figure 5 as transitions (1) and (2), respectively). The initial state for both transitions (1) and (2) has a Ag(I) character (mostly $4d_{yz}$) while the final state has a NO character that consists of a linear combination of the $2p_x$ orbitals in the case of MLCT1 and the $2p_y$ orbitals in the case of MLCT2. These two transitions have been studied by the extended Hückel method as a function of the NO−NO distance in the monomer model shown in Chart 1a. Figure 6 shows a potential energy diagram of the ground state and the two excited states that correspond to the aforementioned transitions. In the calculations, the distance between the two NO molecules was varied while keeping the other distances constant at the values shown in Table 1. The total one-electron energy was plotted in Figure 6 as a function of the NO−NO distance. The results of extended Hückel calculations for the ground and excited states of the monomer model are summarized in Table 3. According to Figure 6, the MLCT1 excited state shows a much deeper well and a much shorter equilibrium distance than the MLCT2 excited state. Furthermore, Table 3 suggests that the MLCT1

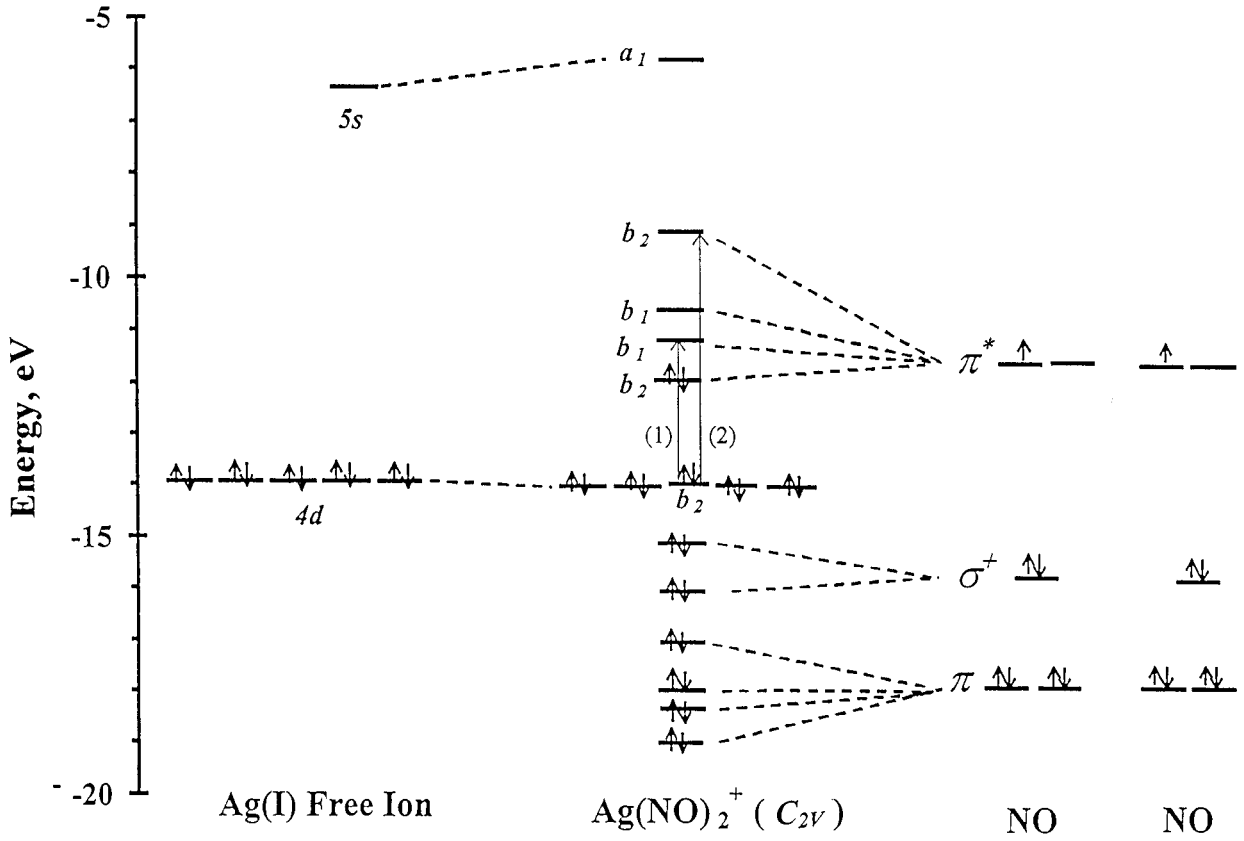

Figure 5. A partial energy level diagram showing the electronic structure of the $Ag(NO)_2^+$ model shown in Chart 1a minimized by extended Hückel calculations.

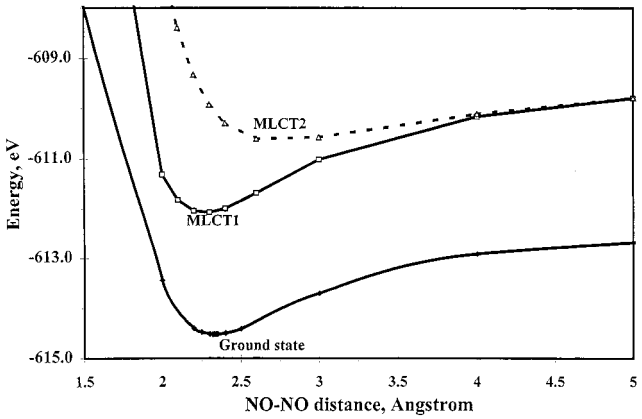

Figure 6. Potential energy diagram of the ground and excited states of the $Ag(NO)_2^+$ model shown in Chart 1a.

transition leads to a shorter NO−NO equilibrium distance, stronger N−N and O−O bonding, and weaker N−O bonding relative to the ground state. In contrast, the MLCT2 transition leads to a longer NO−NO equilibrium distance, and weaker N−N and O−O bonding relative to the ground state. Therefore, both Figure 6 and Table 3 indicate that the photoreaction described in eq 4 is more likely to occur via the MLCT1 transition than the MLCT2 transition in monomer sites of Ag(I) ions.

The electronic structure of the model $[Ag(NO)_2^+]_2$ shown in Chart 1b has been studied in order to understand the influence of argentophilic attraction in the zeolite lattice on the photocatalytic activity for nitric oxide decomposition. The structure of each $[Ag(NO)_2^+]$ unit in the dimer model is the same as that in the minimized structure of the ground state of the monomer model as described above. Therefore, the intraionic NO−NO distance in each $[Ag(NO)_2^+]$ unit was kept constant while varying the distance between the two monomers. The lowest-energy MLCT transition in the model $[Ag(NO)_2^+]_2$ has been studied as a function of the Ag−Ag distance (which is the same as the NO−NO interionic distance). Figure 7 and Table 4 summarize the results of extended Hückel calculations for the ground and the aforementioned excited state for the $[Ag(NO)_2^+]_2$ model. It is evident from Figure 7 that the ground state has a rather shallow potential well. This suggests that the interionic N−N and O−O bonding is rather weak in the ground state (compare with the potential well of the ground state in Figure 6). Obviously, the weak argentophilic attraction in the ground state does not enhance the interionic N−N and O−O bonding significantly (note that Table 4 shows that the total energy is stabilized by <0.06 eV in the ground-state dimer relative to the corresponding monomer).

In contrast to the ground state, the excited state of the $[Ag(NO)_2^+]_2$ model shown in Figure 7 is strongly bonding as evidenced by the rather deep potential well (0.72 eV) and the

TABLE 2: Tentative Assignment of the Luminescence Bands of Ag(I)/ZSM-5 Zeolite

luminescence band	λ_{em}, nm	assignment[a]
A	270−290	$*[Ag^+]_2$
B	310−370	$*[Ag^+]_3$ - angular
C	380−420	$*[Ag^+]_3$ − linear
D,E,F	450−690	delocalized exciplexes[b]

[a] The peaks that appear within each luminescence band (see Figure 2) are due to the cluster ions present in different environments in the zeolite lattice, for example in major channels, minor channels, and surface sites. [b] Bands D−F are collectively labeled as delocalized exciplexes due to $*[Ag^+]_n$ species with $n > 3$. The number of isomers of a given oligomer with $n > 3$ is too large to give a definite assignment for the cluster size.

TABLE 3: Summary of the Results of Extended Hückel Calculations for the Minimized Structures of the $Ag(NO)_2^+$ Model Shown in Chart 1a[a]

electronic state	NO−NO dist, Å	tot energy, eV	bind energy, eV	O.P. (N−N)	O.P. (O−O)	O.P. (N−O)
ground state	2.33	−614.517	2.325	0.1957	0.0255	1.1723
MLCT1	2.27	−612.079	2.713	0.2426	0.0302	1.0213
MLCT2	2.74	−610.646	1.300	0.0365	0.0074	1.0072

[a] O.P., overlap population.

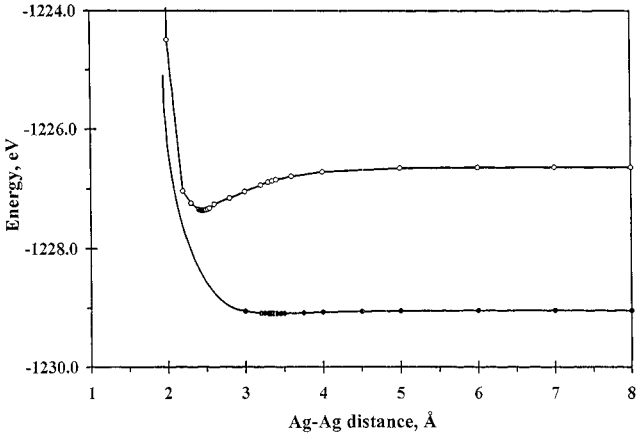

Figure 7. Potential energy diagram of the ground and excited states of the $[Ag(NO)_2^+]_2$ models shown in Chart 1b.

short Ag−Ag equilibrium distance (2.45 Å, which is 0.90 Å shorter than the corresponding ground-state distance). Furthermore, Table 4 shows that the overlap population increases drastically in the excited state relative to the ground state. For example, the intermolecular N−N bonding increases by 2 orders of magnitude while the O−O overlap population becomes positive in the excited state relative to the ground state. Table 4 shows that the increased interionic N−N and O−O bonding in the excited state occurs at the expense of the intraionic bonding of not only N−N and O−O bonds, but also the N−O bonds. These results suggest that oligomerization increases the likelihood for the photoreaction shown in eq 4. We believe that the strong propensity of Ag(I) ions to form excimers[41] provides an additional driving force for the photodecomposition of nitric oxide on the ZSM-5 surface. Table 4 shows that the binding energy is an order of magnitude higher in the excited state relative to the ground state. Similar results have been reported for the $*[Ag(CN)_2^-]_2$ excimers, which have stabilization energies that are also an order of magnitude higher than the corresponding ground-state dimers.[41]

The conclusions drawn from extended Hückel calculations are supported by ab initio calculations at the Hartree−Fock level. Figure 8 shows the surfaces of the HOMO and LUMO for the same $[Ag(NO)_2^+]_2$ dimer model used in the aforementioned extended Hückel calculations. The HOMO is clearly antibonding with respect to interionic N−N, O−O, and Ag−Ag bonds while the LUMO is bonding for these bonds. This suggests that photoexcitation that results in the HOMO → LUMO transition in the $[Ag(NO)_2^+]_2$ should lead to the photoreaction described in eq 4. The same conclusion was reached by extended Hückel calculations but for a different transition with a MLCT character, which is not the HOMO → LUMO transition. This discrepancy is attributed to the fact that the ab initio and extended Hückel calculations we used have different basis sets. Only the valence orbitals of the Ag(I) ion (4d, 5s, 5p) were used in the extended Hückel calculations. The inclusion of the core electrons in the basis sets of the Hartree−Fock calculations increases the likelihood for mixing between the Ag(I) orbitals and the NO orbitals. Nevertheless, both methods support the conclusion that dimerization of the $Ag(NO)_2^+$ ion provides an additional route for the photodecomposition of NO by Ag(I) ions.

Extended Hückel calculations suggest that intraionic bonding in $[Ag(NO)_2^+]$ contributes to nitric oxide decomposition. However, in the $[Ag(NO)_2^+]_2$ model both interionic and intraionic bonding exist so it is desired to study the influence of interionic bonding only. We have considered a new model by the ab initio method because this method is more realistic and also because the extended Hückel program in our hands does not allow us to include too many atoms with a complicated geometry. Figure 9 shows the model we used to study interionic Ag−Ag bonding. The model shown in Figure 9 has two adjacent Ag(I) ions surrounded by O atoms in a plane similar to the oxide environment of the zeolite ring. A nitric oxide molecule is adsorbed on each Ag(I) ion in a geometry perpendicular to the plane of the simulated zeolite ring.[53] The bonding between the N−N and O−O atoms in the LUMO of the model is unmistakable according to Figure 9. The HOMO, on the other hand, is antibonding with respect to Ag−Ag, N−N, and O−O bonds. This result suggests that the adsorption of NO molecules on adjacent Ag(I) ions may lead to eq 4 even if only one NO molecule is adsorbed on each Ag(I) ion.

Discussion

1. Assignment of the Luminescence Bands. A previous study has reported one emission band at ∼350 nm using 220 nm excitation (band B in Table 2). The authors have attributed this band to Ag(I) monomers in the ZSM-5 zeolite lattice.[18] The lowest singlet excited state of a free Ag(I) ion ($^1D_2$) lies some 46 000 cm^{-1} above the ground electronic state.[60] The 350 nm emission is >17 000 cm^{-1} lower in energy than the energy of the $^1D_2$ state of Ag(I). Obviously, this red shift is too large to be attributed to monomer emission. We have carried out Hartree−Fock ab initio calculations for a single Ag(I) ion at the center of the simulated zeolite lattice described in ref 53. The results indicate that the energy of the lowest-energy 4d−5s transition of the Ag(I) ion in the zeolite environment is ∼53 × 10^3 cm^{-1}. The highest-energy excitation band for the Ag(I)/ZSM5 system occurs at ∼220 nm, some 8 × 10^3 cm^{-1} lower in energy than the 4d−5s transition obtained by the ab initio calculations. The singlet−triplet splitting for an Ag(I) ion is also about 8 × 10^3 cm^{-1}. Therefore, it is reasonable to assume that the 220 nm band observed in the excitation spectra of the Ag(I)/ZSM5 system is due to the 4d−5s singlet-to-triplet transition of the Ag(I) monomer ion. The absorption edge of the Ag(I)/ZSM5 system is also observed at ∼220 nm.[18] The emission bands of the Ag(I)/ZSM5 system have much lower energies than the energy of the 4d−5s singlet-to-triplet transition. For example, even the highest-energy emission band A is some 1.1 × 10^4 cm^{-1} lower in energy than the absorption band. Therefore, the luminescence bands do not originate from monomer Ag(I) ions. Instead, excitation of Ag(I) ions is followed by energy transfer to $*[Ag]_n$ oligomer ions with $n \geq 2$. Energy transfer from monomer sites to oligomer sites explains

TABLE 4: Summary of the Results of Extended Hückel Calculations for the Minimized Structures of the $[Ag(NO)_2^+]_2$ and $[Ag(NO)_2^+]_3$ Models Shown in Chart 1[a]

electronic state	Ag−Ag Dist,[b] Å	tot energy, eV	bind energy, eV	O.P. (Ag−Ag)	O.P. (N−N)[c]	O.P. (O−O)[d]	O.P. (N−N)[d]	O.P. (O−O)[d]	O.P. (N−O)[d]
grd−dimer	3.35	−1229.091	0.057	−0.0106	0.0007	−0.0004	0.1960	0.0255	1.1723
exc−dimer	2.45	−1227.358	0.723	+0.0157	0.0970	+0.0051	0.1743	0.0167	1.0948
grd−dimer	3.29	−1843.69	0.135	−0.0149	+0.0009	−0.0005	−0.0603	0.0255	1.1730
exc−dimer	2.74	−1843.41	0.604	−0.0229	0.0327	0.0011	0.1673	0.0149	1.1428

[a] O.P., overlap population. [b] Same as the interionic NO−NO distance. The intraionic NO−NO distance was held constant at the value that corresponds to the minimized structure of the ground state of the monomer model. [c] Interionic (between the NO molecules of the two adjacent $Ag(NO)_2^+$ monomer units). [d] Intraionic (between the NO molecules of the same $Ag(NO)_2^+$ monomer unit).

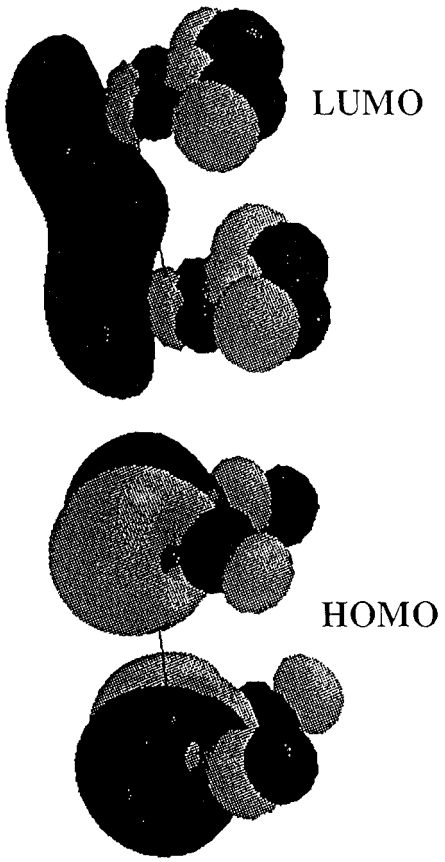

Figure 8. Surfaces of the HOMO (bottom) and LUMO (top) as depicted from ab initio calculations for the $[Ag(NO)_2^+]_2$ model shown in Chart 1b. Note that the N−N, O−O, and Ag−Ag bonding character is antibonding in the HOMO and bonding in the LUMO.

the strong luminescence from oligomer centers even if the number of oligomers is far less than the number of monomers (as expected statistically).

In a recent study, Omary et al. have suggested that two types of mechanisms are responsible for the emission bands of Ag(I) complexes that exhibit multiple luminescence centers: direct excitation and energy transfer.[61] A similar argument applies herein because the luminescence bands of Ag(I)/ZSM-5 are similar to those exhibited by $Ag(CN)_2^-$/KCl crystals.[41,61] Therefore, energy transfer from monomers to dimers and trimers explains the luminescence bands A and B upon excitation with 220 nm. Direct excitation occurs upon using longer excitation wavelengths. The luminescence bands are assigned to $*[Ag^+]_n$ oligomers that differ in "*n*" and/or configuration. Individual peaks within the major emission and excitation bands are most likely due to the presence of Ag(I) oligomer ions in different environments in the ZSM-5 zeolite host. In Table 2, tentative assignments of the luminescence bands are given. Accurate assignments are not possible in the absence of direct structural data such as X-ray crystallography, so the assignments in Table 2 are qualitative.

The individual peaks within each luminescence band are due to the presence of $[Ag^+]_n$ oligomers in different environments and/or to different geometrical isomers of a given oligomer (e.g., the $[Ag^+]_3$ trimer can be either linear or angular). The synchronous-scan spectra in Figure 2 show the individual peaks within the luminescence bands more clearly and more than 10 peaks have been obtained (vide supra). Such a high resolution observed in the synchronous-scan spectra is rarely observed in conventional emission spectra without using powerful laser sources. The appearance of these peaks in Figure 2 underscores the presence of several environments of Ag(I) ions in the ZSM-5 lattice. The $[Ag^+]_n$ oligomers can be located in major channels, minor channels, as well as on the surface of the ZSM-5 substrate. Changing the temperature may alter this distribution, as Figure 3a suggests. For example, note in Figure 3a the appearance of distinct peaks on the high-energy side of band B and the increase in the intensity ratio of the higher-energy component in band C as temperature is increased. Changing the temperature also affects the energy transfer processes between the different $*[Ag^+]_n$ species, which leads to changes in the intensity ratios of the different luminescence bands. Note in Figure 3b that the luminescence band at ~350 nm (B) is quenched while the lower-energy bands are enhanced as a result of an increase in temperature. This result is explained in terms of a thermally activated energy transfer process from excitons characteristic of band B to lower-energy excitons.

Since the luminescence of d^{10} systems has a demonstrated sensitivity toward metal−metal interactions, different emissions are expected to occur from various Ag centers in the zeolite. The luminescence spectra suggest the presence of multiple aggregations of the Ag(I) ions in the ZSM-5 host. The highest-energy emission (band A) near 280 nm region is attributed to a $*[Ag^+-Ag^+]$ excimer. The photoluminescence bands at 310−370 nm (band B) and at 380−420 nm (band C) are attributed to two geometrical isomers of a $*[Ag^+]_3$ trimer exciplex. The Ag atoms are distributed in a linear arrangement ($D_{\infty h}$) in one trimer (band C) and in an angular arrangement (C_{2v}) in the other isomer (band B). The luminescence bands A, B, and C of the Ag(I)/ ZSM-5 system (Figure 1) are similar in shapes and energies to those exhibited by $[Ag(CN)_2^-]$/KCl doped crystals.[41] Therefore, a similar assignment is used in Table 2 for these bands. The longer wavelength bands of the Ag(I)/ ZSM-5 catalyst are attributed to $*[Ag^+]_n$ delocalized exciplexes with $n > 3$, as shown in Table 2. These results are reminiscent of the "exciplex tuning" phenomenon which has been reported recently for doped crystals of $[Ag(CN)_2^-]$/KCl.[41]

2. Active Catalytic Sites in Ag(I)/ZSM-5. UV irradiation of the Ag(I)/ZSM-5 catalyst in the presence of 10 Torr NO at 298 K leads to decomposition of NO into N_2, N_2O, and NO_2.[18] The data in this study also suggest that all luminescent centers of the Ag(I)/ZSM-5 sample have excitation peaks in the UV

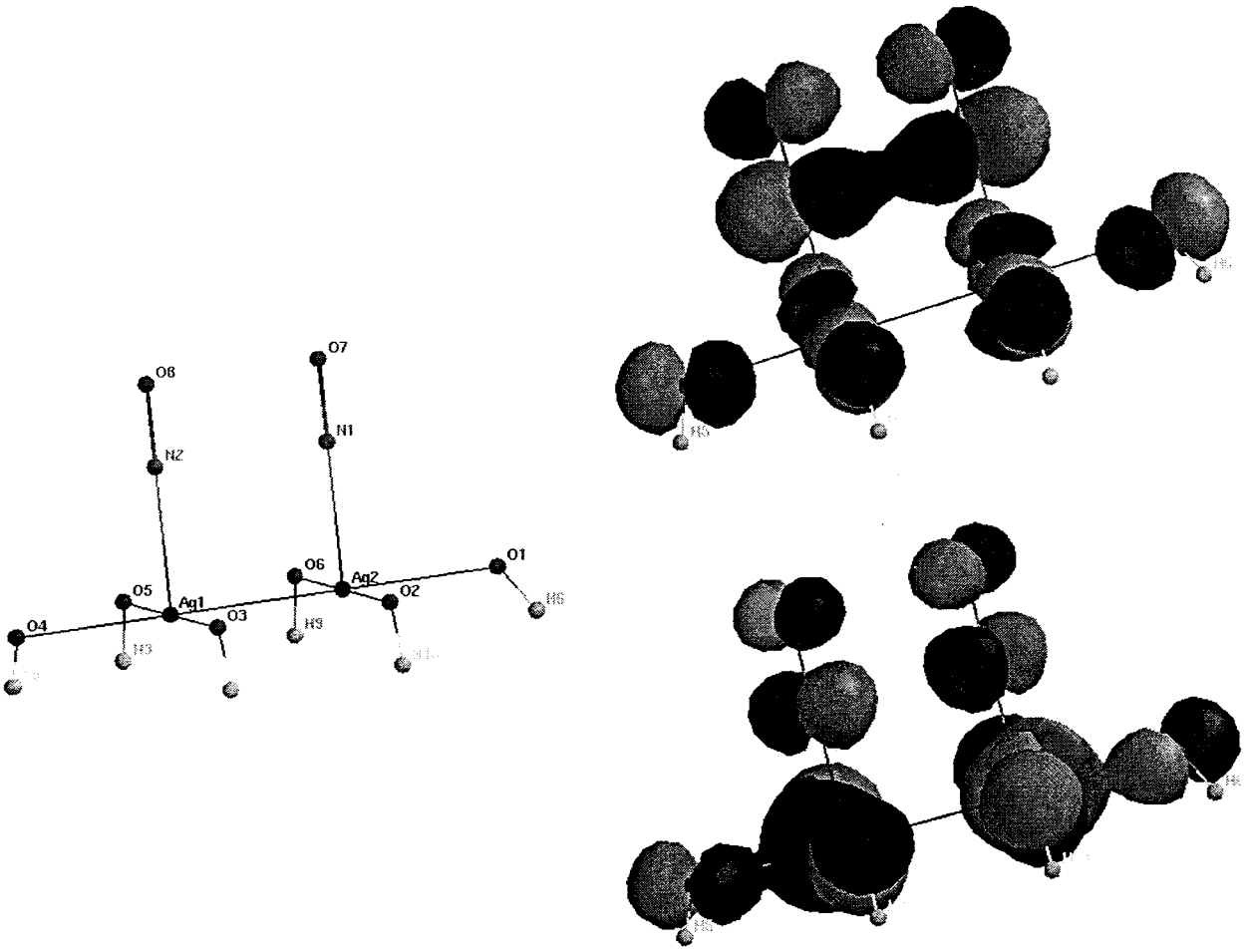

Figure 9. Surfaces of the HOMO (bottom) and LUMO (top) as depicted from ab initio calculations for a model for Ag(I) ions in an oxide environment. Note that the N−N, O−O, and Ag−Ag bonding character is antibonding in the HOMO and bonding in the LUMO.

region that overlap with the wavelengths of the high-pressure mercury lamp used for the photocatalytic study (see Table 2). This includes isolated Ag(I) ions as well as $[Ag^+]_n$ oligomers. The theoretical calculations described above suggest that isolated ions and oligomers of Ag(I) ions in the ZSM-5 lattice bothrepresent active sites for the photocatalytic decomposition of nitric oxide.

The data in the present study underscore the existence of $[Ag^+]_n$ oligomers and not just isolated Ag(I) ions. In addition to the strong spectroscopic and theoretical evidence discussed above, the structural EXAFS data are also in support of this conclusion. The phase-uncorrected EXAFS peaks of Ag_2O at 1.8 and 3.5 Å (corresponding to crystallographic values of 2.05 and 4.1 Å, respectively)[57−59] are attributed to Ag−O and Ag−O−Ag bonding while the peak of the Ag foil at 2.5 Å (2.88 Å crystallographic value)[57−59] is due to Ag−Ag bonding. The EXAFS of the Ag(I)/ZSM-5 catalyst exhibits peaks corresponding to Ag−O and Ag−Ag bonding (Trace I in Figure 4). The observation of the Ag−Ag EXAFS peak is indicative of oligomerization of Ag(I) ions in the ZSM-5 lattice. Yokoyama et al. have reported EXAFS data of Ag clusters in SiO_2, in which Ag−Ag peaks are observed at the same location of the Ag(I)/ZSM EXAFS peak we assign herein to Ag−Ag bonding.[58] It should be noted that the intensity of the EXAFS peak for the Ag(I)/ZSM-5 catalyst near 2.5 Å is quite weak (∼2% the intensity of the corresponding peak in the Ag foil, which has a coordination number of 12). This may be indicative that the majority of the Ag species in the catalyst are Ag(I) monomers, while the $[Ag^+]_n$ oligomers are minor species. However, one should keep in mind that weak interactions, such as the Ag(I)−Ag(I) closed-shell (d^{10}−d^{10}) interactions cannot be detected easily by EXAFS at room temperature.[62] The reason for this little sensitivity is the high values of the Debye−Waller and backscattering factors in such cases, which dampen the EXAFS signal amplitude, as demonstrated in several EXAFS studies of Ag(I)[59,63] and Au(I)[64] materials. The fact that EXAFS peaks due to Ag−Ag bonding are detected for the Ag(I)/ZSM-5 catalyst (Figure 4) despite the little sensitivity of the method counteracts the low intensity of the peak.

Figure 4 indicates that the peak seen near 3.5 Å for Ag_2O is virtually absent in the EXAFS spectrum of the Ag(I)/ZSM-5 sample, indicating the absence of significant Ag−O−Ag bonding. This result suggests that the oligomerization of Ag(I) ions most likely exists in the same zeolite ring as opposed to oligomerization between ions in adjacent rings with O atoms bridging the Ag(I) ions. Figure 9 suggests that oligomerization between Ag(I) ions without O bridges may lead to the desired photocatalytic reaction. In fact, we have attempted to model Ag−Ag bonding with oxygen atoms bridging the Ag(I) ions between different zeolite rings. However, the surfaces of the frontier orbitals obtained by ab initio calculations have indicated that these sites cannot catalyze the photoreaction in eq 4. We conclude that $[Ag^+]_n$ oligomers exist in the zeolite lattice with Ag−Ag bonding occurring without the assistance of bridging oxygen atoms from the silicates or aluminates.

On the basis of structural and spectroscopic data in this study, we postulate in Figure 10 a possible geometry for $[Ag^+]_n$ oligomers within the zeolite lattice. All interatomic

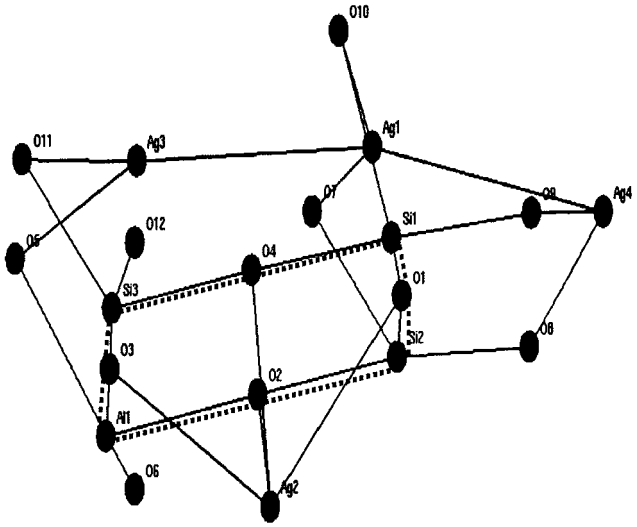

Figure 10. A computer graphic showing a possible geometry for $[Ag^+]_n$ oligomers within the ZSM-5 zeolite lattice. The dimensions of the ZSM-5 zeolite ring are according to ref 53. Examples of some interatomic distances (Å): Ag1−Ag2 = 3.104; Ag1−Ag3 = 3.000; Ag1−Ag4 = 3.000; Ag2−Ag3 = 3.295; Ag3−O5 = 2.100; Ag4−O9 = 2.254; Ag1−O7 = 2.563; Ag3−O7 = 3.082; Ag3−O10 = 3.915.

distances in Figure 10 agree with published values for similar systems.[48,58,65−66] All Ag(I) ions are separated by distances in the range 3.0−3.4 Å, the typical range reported for Ag(I) species in oxide environments. The Ag(I) ion labeled as "Ag2" in Figure 10 is drawn below the plane of the zeolite ring because the ring cannot fit an Ag(I) ion given the Ag−O separations published in the literature (2.1−2.6 Å). Each of the Ag(I) ions above the plane of the zeolite ring is coordinated directly to two oxygen atoms with Ag−O distances in the 2.1−2.6 Å range. The oxygen atoms coordinated to a given Ag(I) ion are separated by very long distances (>3 Å) from other adjacent Ag(I) ions, thus precluding the bridging role of these oxygen atoms as dictated by the EXAFS data. The model shown in Figure 10 is realistic because many examples have been reported in the literature for Ag(I) ions present in aggregations within oxide environments.[48,58,65,66] For example, Jansen and Linke have reported the presence of octahedral aggregations of silver between the tetrahedral units of silicates and germanates.[65,66] The crystal structures of these compounds show Ag−Ag distances of ∼3.0−3.3 Å with no Ag−O−Ag bridging. That is, Ag−Ag bonding on the upper van der Waals level is quite common in Ag(I) species in oxide materials such as silicates and germanates. Silver clusters in anchored zeolites have been synthesized and characterized by X-ray diffraction,[67] EPR,[68] and far-infrared techniques.[69] For example, the structure of Ag(I)-exchanged zeolite A has Ag atoms forming a linear trimer with Ag−Ag distances of 2.85−3.00 Å, and each cuboctahedron of zeolite A can accommodate up to four silver trimers.[67]

Occupation of the Ag sites in a structure similar to the one in Figure 10 is a function of the Ag loading in the ZSM-5 lattice. As a result, a zeolite ring like the one shown in Figure 10 may contain isolated Ag(I) ions in one extreme case, $[Ag^+]_4$ oligomers in another case. Isolated ion sites would show no luminescence. Filling two of the four Ag sites would lead to the A emission. If three Ag sites were filled, the observed luminescence would depend on which sites are filled. For example, filling the sites (Ag3, Ag1, Ag4) and (Ag1, Ag2, Ag3) would lead to the emission bands C and B, respectively. If all four sites (or more) were filled, lower-energy emissions such as band E would be observed. Our experience with Ag(I) species in alkali halide matrices suggests that the silver loading in the ZSM-5 sample used in this study is high enough to produce a distribution of $[Ag^+]_n$ oligomers that leads to the luminescence bands observed herein.[41,61] We conclude that Figure 10 is a reasonable model for the structure of Ag(I)/ZSM-5 based on the experimental and theoretical data in this study, which are supported by structural data reported in the literature for similar systems.

SCHEME 1

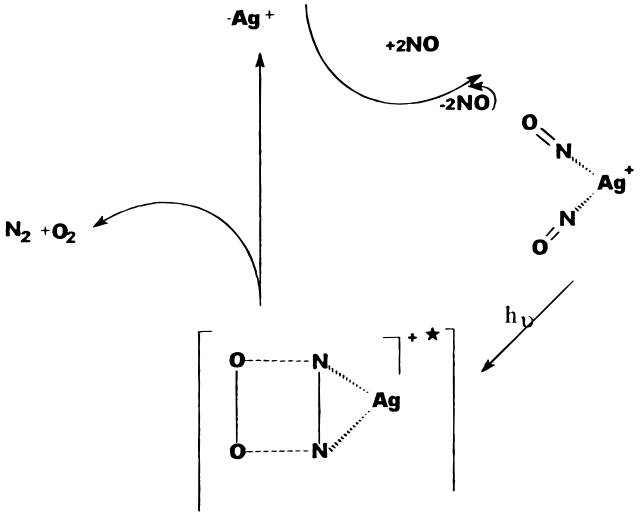

SCHEME 2

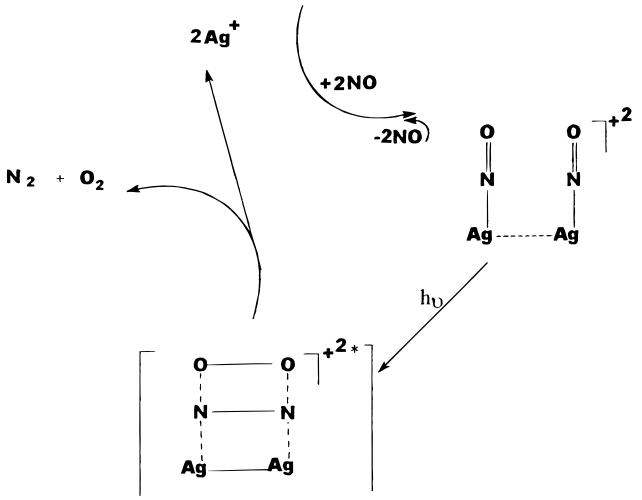

3. Photocatalytic Models. From the experimental and theoretical results discussed above, two pathways are proposed to explain the NO decomposition into N_2 and O_2 on the Ag(I)/ZSM-5 surface. The first pathway proceeds through $Ag(NO)_2^+$ (Scheme 1) and the second pathway proceeds through the $[Ag(NO)]_2^{2+}$ dimer (Scheme 2).

The first pathway involves the adsorption of two NO molecules on the Ag(I) site to give $Ag(NO)_2^+$. UV irradiation of $Ag(NO)_2^+$ gives an intermediate in which the N−O and Ag−N bonds are antibonding whereas, the N−N and O−O bonds are bonding. As a result, NO molecules adsorbed on Ag(I) monomer sites dissociate to produce N_2 and O_2. The photocatalytic cycle for the predicted mechanism is illustrated in Scheme 1.

The second type of mechanism involves the formation of an excimer $*[Ag(NO)]_2^{2+}$ upon the UV irradiation of the $[Ag(NO)]_2^{2+}$ dimer. In this excimer the Ag−Ag, N−N, and O−O

bonding is much stronger than in the ground state. Photodecomposition of this excimer will produce N_2 and O_2. The photocatalytic cycle for the predicted mechanism is illustrated in Scheme 2. The Ag−Ag bonding in the excited state provides an additional driving force for this photoreaction. That is, the formation of a $*[Ag(NO)]_2^{2+}$ excimer provides a metastable excited state that may act as an intermediate for the decomposition of nitric oxide. We should point out that our results also show that Ag−Ag bonding is not limited to dimer sites. The luminescence results indicate that the trimer exciplexes $*[Ag^+]_3$ as well as longer-chain exciplexes are also present in the Ag(I)/ZSM-5 catalyst (see Table 2). Therefore, it is likely that $*[Ag(NO)^+]_3$ exciplexes may form upon the introduction of NO gas to the catalyst followed by photoexcitation. In fact, it has been recently reported that the aggregation of Ag(I) species is a favorable process that is strengthened in the excited state.[40,41,48] We conclude that Ag−Ag bonding in the excited state provides intermediates for the photodecomposition of NO on the Ag(I)-doped ZSM-5 catalyst.

Conclusions

The photocatalytic decomposition of NO on the surface of Ag(I)-doped ZSM-5 zeolite occurs in catalytic sites of the Ag(I) ions. Conventional and synchronous-scan photoluminescence results underscore the presence of multiple environments of Ag(I) ions. Theoretical calculations suggest that several monomeric and oligomeric models of $[Ag_n(NO)_m]_n^+$ ($n = 1-3$, $m = 1,2$) can act as reactive sites for the photodecomposition of nitric oxide into nitrogen and oxygen. The reactive excited states have been characterized as ones in which N−N, O−O, and Ag−Ag bonding interactions are present. The $*[Ag(NO)^+]_2$ excimers and $*[Ag(NO)^+]_3$ exciplexes have been suggested as intermediates in the photocatalytic cycle. The increased stability of the excited state as a result of Ag−Ag bonding provides a driving force for the photodecomposition of NO into N_2 and O_2 on the surface of Ag(I)-doped ZSM-5 zeolite in catalytic sites of the Ag(I) ions.

Acknowledgment. Acknowledgment is made to the donors of the Petroleum Research Fund, administered by the American Chemical Society, for the support of this research. M.A.O. acknowledges an Academic Research Infrastructure Grant (No. 9512457) from the National Science Foundation and a grant from Paul J. Schupf for the Paul J. Schupf Scientific Computing Center at Colby College.

References and Notes

(1) Yamashita, H.; Ichihashi, Y.; Anpo, M.; Hashimoto, M.; Louis, C.; Che, M. *J. Phys. Chem*. **1996**, *100*, 16041.
(2) Anpo, M.; Ichihashi, Y.; Takeuchi, M.; Yamashita, H. *Res. Chem. Intermed*. **1998**, *24*, 143.
(3) Anpo, M.; Yamashita, H.; Ikeue, K.; Fujii, Y.; Ichihashi, Y.; Zhang, S.; Park, D.; Ehara, S.; Park, S.; Chang, J.; Yoo, J. *Surf. Sci. Catal*. **1998**, *114*, 177.
(4) Yamashita, H.; Kawasaki, S.; Ichihashi, Y.; Harada, M.; Takeuchi, M.; Anpo, M. *J. Phys. Chem. B* **1998**, *102*, 5870.
(5) Anpo, M.; Yamashita, H.; Ichihashi, Y.; Fujii, Y.; Honda, M. *J. Phys. Chem. B* **1997**, *101*, 2632.
(6) Yamashita, H.; Kawasaki, S.; Takeuchi, M.; Fujii, Y.; Ichihashi, Y.; Suzuki, Y.; Park, S.; Chang, J.; Yoo, J.; Anpo, M. *Surf. Sci. Catal*. **1998**, *114*, 561.
(7) Yamashita, H.; Ichihashi, Y.; Zhang, S.; Matsumura, Y.; Souma, Y.; Tatsumi, T.; Anpo, M. *Appl. Surf. Sci*. **1997**, *121/122*, 305.
(8) Anpo, M. *Protecting Environ*. **1998**, 75.
(9) Anpo, M.; Tomonari, M.; Fox, M. *J. Phys. Chem*. **1989**, *93*, 7300.
(10) Anpo, M.; Kawamura, T.; Kodama, S.; Maruya, K.; Onishi, T. *J. Phys. Chem*. **1988**, *92*, 438.
(11) Anpo, M.; Shima, T.; Kodama, S.; Kubokawa, Y. *J. Phys. Chem*. **1987**, *91*, 4305.
(12) Zhang, S.; Higashimoto, S.; Yamashita, H.; Anpo, M. *J. Phys. Chem*. **1998**, *102*, 5590.
(13) Anpo, M.; Sunamoto, M.; Che, M. *J. Phys. Chem*. **1989**, *93*, 1187.
(14) Anpo, M.; Sunamoto, M.; Fujii, T.; Patterson, H. H.; Che, M. *Res. Chem. Intermed*. **1989**, *11*, 245.
(15) Anpo, M.; Kondo, M.; Coluccia, S.; Che, M. *J. Am. Chem. Soc*. **1989**, *111*, 8791.
(16) Louis, C.; Che, M.; Anpo, M. *J. Catal*. **1993**, *141*, 453.
(17) Anpo, M.; Matsuoka, M.; Yamashita, H. *Catal. Today* **1997**, *35*, 177.
(18) Anpo, M.; Zhang, S.; Mishma, H.; Matsuoka, M.; Yamashita, H. *Catal. Today* **1997**, *39*, 159.
(19) Anpo, M. *IL. Nuovo. Cimento* **1997**, *19*, 1641.
(20) Matsuoka, M.; Matsuda, E.; Tsuji, K.; Yamashita, H.; Anpo, M. *J. Mol. Catal. A., Chem*. **1996**, *107*, 399.
(21) Anpo, M.; Matsuoka, M.; Hanou, K.; Mishima, H.; Yamashita, H.; Patterson, H. H. *Coord. Chem. Rev*. **1998**, *171*, 175.
(22) Yamashita, H.; Matsuoka, M.; Tsuji, K.; Shioya, Y.; Anpo, M.; Che, M. *J. Phys. Chem*. **1996**, *100*, 397.
(23) Anpo, M.; Matsuoka, M.; Mishima, H.; Yamashita, H. *Res. Chem. Intermed*. **1997**, *23*, 197.
(24) Blint , R. J. *J. Phys. Chem*. **1996**, *100*, 19518.
(25) Mohamed, M.; Vansant, E. *J. Mater. Sci*. **1995**, *30*, 4834.
(26) Li, Y.; Hall, K. W. *J. Phys. Chem*. **1990**, *94*, 6145.
(27) Valyon, J.; Hall, K. W. *J. Phys. Chem*. **1993**, *97*, 1204.
(28) Centi, G.; Perathoner, S.; Shioya, Y.; Anpo, M. *Res. Chem. Intermed*. **1992**, *17*, 125.
(29) Beer, R.; Calzaferri, G.; Kamber I. *J. Chem. Soc., Chem. Commun*. **1991**, 1489.
(30) Iwamoto, M.; Yokoo, M.; Sakai, K.; Kagawa, S. *J. Chem. Soc., Faraday Trans. 1* **1981**, *77*, 1629.
(31) Iwamoto, M.; Furukawa, H.; Kagawa, S. *Chem. Lett*. **1986**, *28*, 943.
(32) Iwamoto, M.; Hamada, H. *Catal. Today* **1991**, *10*, 57.
(33) Shelef, M. *Catal. Lett*. **1992**, *15*, 305.
(34) Fox, M. A. *Res. Chem. Intermed*. **1991**, *15*, 153.
(35) Anpo, M.; Matsuoka, M.; Shioya, Y.; Yamashita, H.; Giamello, E.; Morterra, C.; Che, M.; Patterson, H. H.; Webber, S.; Ouellette, S.; Fox, M. A. *J. Phys. Chem*. **1994**, *98*, 5744.
(36) Fortin, D.; Drouin, M.; Turcotte, M.; Harvey, P. D. *J. Am. Chem. Soc*. **1997**, *119*, 531.
(37) Vogler, A.; Kunkely, H. *Chem. Phys. Lett*. **1989**, *158*, 74.
(38) Henary, M.; Zink, J. I. *Inorg. Chem*. **1991**, *30*, 3111.
(39) Omary, M. A.; Patterson, H. H.; Shankle. G. *Mol. Cryst. Liq. Cryst*. **1996**, *284*, 399.
(40) Omary, M. A.; Patterson, H. H. *Inorg. Chem*. **1998**, *37*, 1060.
(41) Omary, M. A.; Patterson, H. H. *J. Am. Chem. Soc*. **1998**, *120*, 7696.
(42) von der Austin, W.; Stolz, H. *J. Phys. Chem. Solids* **1990**, *51*, 765.
(43) Hamilton, J. F. *Adv. Phys*. **1988**, *37*, 359.
(44) Ueta, M.; Kanzaki, H.; Kabayashi, K.; Toyozawa, Y.; Hanamura, E. *Excitonic Processes in Solids*; Springer: Berlin, 1986; pp 309−69.
(45) (a) Moser, F.; Barkay, N.; Levite, A.; Margalit, E.; Paiss, I.; Sa′ar, A.; Schnitzer, I.; Zur, A.; Katzir, A. *Proc. SPIE* **1990**, *128*, 1228. (b) Baetzold, R. C. *J. Phys. Chem. B* **1997**, *101*, 8180.
(46) (a) Meijerink, A.; van Heek, M. E.; Blasse, G. *J. Phys. Chem. Solids* **1993**, *54*, 901. (b) Mesnaoui, M.; Maazaz, M.; Parent, C.; Tanguy, B.; LeFlem, G. *Eur. J. Solid State Inorg. Chem*. **1992**, *29*, 1001.
(47) Köhler, B. U.; Weppner, W.; Jansen, M. *J. Solid State Chem*. **1985**, *57*, 227.
(48) For a review see: Jansen, M. *Angew. Chem*. **1987**, *99*, 1136; *Angew. Chem., Int. Ed. Engl*. **1987**, *26*, 1098.
(49) Omary, M.; Patterson, H. Electronic Spectroscopy: Luminescence Theory. *Encyclopedia of Spectroscopy & Spectrometry*; Academic Press: London, U.K.; 1999.
(50) Shin, K. K.; Barrie, J. D.; Dunn, B.; Zink, J. I. *J. Am. Chem. Soc*. **1990**, *112*, 5701.
(51) Tanaka, T.; Yamashita, H.; Tsuchitani, R.; Funabiki, T.; Yoshida, S. *J. Chem. Soc., Faraday Trans. 1* **1988**, *84*, 2987.
(52) Pyykkö, P.; Lohr, L. L. *Inorg. Chem*. **1981**, *20*, 1950.
(53) Zhanpeisov, N. U.; Nakatsuji, H.; Hada, M.; Nakai, H.; Anpo, M. *Catal. Lett*. **1996**, *42*, 173.
(54) Taylor, T.; Patterson, H. H. *Anal. Chem*. **1987**, *59*, 2180.
(55) MacDonald, B. C.; Lvin. S. J.; Patterson, H. H. *Anal. Chim. Acta* **1997**, *338*, 155.
(56) Wang, X.; Bartha, R. *Environ. Sci. Technol*. **1990**, *24*, 1086.
(57) Houde-Walter, S. N.; Inman, J. M.; Dent, A. J.; Greaves, G. N. *J. Phys. Chem*. **1993**, *97*, 9330.
(58) (a) Yokoyama, T.; Ohta, T. *Jpn. J. Appl. Phys*. **1990**, *29*, 2052. (b) Yokoyama, T.; Kimoto, S.; Ohta, T. *Jpn. J. Appl. Phys*. **1989**, *28*, L851.
(59) Hecht, D.; Borthen, P.; Strehblow, H. H. *J. Electroanal. Chem*. **1995**, *381*, 113.
(60) Moore, C. E. *Atomic Energy Levels*; Nat. Bur. Stand.: Washington, DC, 1958; Circ. 467, Vol. III.

(61) Omary, M. A.; Hall, D. R.; Shankle, G. E.; Siemiarczuck, A.; Patterson, H. H. *J. Phys. Chem. B* **1999**, *103*, 3845.

(62) (a) Carr, N.; Crossley, J. G.; Dent, A. J.; Gouge, J. R.; Neville, G.; Jarrett, P. J.; Orpen, A. G. *J. Chem. Soc., Chem. Commun*. **1990**, 1370. (b) Kortright, J. B.; Bienenstock, A. *Phys. Rev. B* **1988**, *37*, 2979.

(63) Mansour, A. N. *J. Phys. Chem*. **1990**, *94*, 1006.

(64) Jones, W. B.; Yuan, J.; Narayanaswamy, R.; Young, M. A.; Elder, R. C.; Bruce, A. E.; Bruce, M. R. M. *Inorg. Chem*. **1995**, *34*, 1996.

(65) Linke, C.; Jansen, M. *Inorg. Chem*. **1994**, *33*, 2614.

(66) Jansen, M.; Linke, C. *Angew. Chem*. **1992**, *104*, 618; *Angew. Chem., Int. Ed. Engl*. **1992**, *31*, 653.

(67) Gellens, L. R.; Mortier, R. A.; Schoonheydt, R. A.; Uytterhoeven, J. B. *J. Phys. Chem*. **1981**, *85*, 2783.

(68) Gachard, E.; Belloni, J.; Subramanian, M. A. *J. Mater. Chem*. **1996**, *6*, 867.

(69) Baker, M. D.; Ozin, G. A.; Godber, J. *J. Phys. Chem*. **1985**, *89*, 305.